New constraints on primordial features from the galaxy two-point correlation function

Mario Ballardini,[1,2,3,4,*] Fabio Finelli,[2,3] Federico Marulli,[1,2,3] Lauro Moscardini,[1,2,3] and Alfonso Veropalumbo[5]

[1]*Dipartimento di Fisica e Astronomia, Alma Mater Studiorum Università di Bologna, via Gobetti 93/2, I-40129 Bologna, Italy*
[2]*INAF/OAS Bologna, via Piero Gobetti 93/3, I-40129 Bologna, Italy*
[3]*INFN, Sezione di Bologna, viale C. Berti Pichat 6/2, I-40127 Bologna, Italy*
[4]*Department of Physics and Astronomy, University of the Western Cape, Cape Town 7535, South Africa*
[5]*Dipartimento di Fisica, Università degli Studi Roma Tre, via della Vasca Navale 84, I-00146 Rome, Italy*

(Received 17 February 2022; accepted 14 February 2023; published 23 February 2023)

Features in the primordial power spectrum represent the imprinted signal in the density perturbations of the physics and evolution of the early Universe. A measurement of such signals will represents the need to go beyond the minimal assumption made for the initial conditions of the cosmological perturbations. For the first time, we study different templates with undamped oscillations or a bump from the two-point correlation function measured from BOSS DR12 galaxies constraining the amplitude of the features to be at most a few percent. Constraints are competitive to the ones obtained with *Planck* DR3.

DOI: 10.1103/PhysRevD.107.043532

I. INTRODUCTION

Measurements of cosmic microwave background (CMB) anisotropies, such as those from *Planck* DR3 [1–3], have contributed significantly to the characterization of the initial conditions of the Universe. The tight CMB constraints to spatial curvature, isocurvature fluctuations, and primordial non-Gaussianity, all agree with predictions of the standard single field slow-roll models [4–10].

While in these simplest realizations the nearly exponential expansion driven by a scalar field ϕ slowly rolling down a sufficiently flat potential $V(\phi)$ predicts a nearly scale-invariant primordial power spectrum (PPS), several classes of inflationary models predict features in the PPS such as scale-dependent oscillations.

Indeed, primordial features (PF) are expected to appear as deviations from a power law in the PPS due to local or nonlocal modifications of the inflaton potential [11–17], to the presence of new interactions and heavy particles [18–22], non-Bunch-Davies initial conditions [23–25], or also as imprints of alternatives to cosmic inflation [21,22,26]. Moreover, phenomenologically they can be connected to persistent anomalies in the CMB temperature angular power spectrum measured by WMAP [27] and by *Planck* observations [2,28,29]; PF have been also proposed to explain anomalies such as the CMB lensing anomaly, the H_0 and the S_8 tensions [2,30–32].

In order to go beyond the current $2\sigma - 3\sigma$ evidence of some PF patterns from CMB anisotropy measurements [2,27–29,33–39], it has been shown how future large-scale structure observations will be able to improve current constraints on these oscillatory-feature models. This will give the opportunity to further investigate the presence of any salient feature in the matter power spectrum, complementing the constraints based on CMB anisotropy measurements to smaller scales, and being very powerful to constrain high-frequency oscillations appearing on the PPS, see Refs. [40–46]. In this perspective, an intensive effort has been put in place to study the nonlinear dynamics of the cold dark matter (CDM) power spectrum for initial conditions containing PF, see Refs. [45–50].

The goal of this work is to provide new constraints on the amplitude of PF for models with superimposed undamped oscillations or a bump performing the first analysis of PF models with the galaxy two-point correlation function (2PCF) from the Sloan Digital Sky Survey III Baryon Oscillation Spectroscopic Survey Data Release 12 (BOSS DR12).

Our paper is organized as follows. After this introduction, we described the primordial feature models and the corresponding PPS templates studied in Sec. II. In Sec. III, we described the datasets considered and the modeling for the 2PCF used for the analysis together with the prior on the cosmological and nuisance parameters in Sec. IV. We present our results obtained with SDSS BOSS DR12 in Sec. V. In Sec. VI, we draw our conclusions.

*mario.ballardini@inaf.it

II. MODELS OF OSCILLATORY PRIMORDIAL POWER SPECTRUM

Starting from the standard power-law PPS of the comoving curvature perturbations $\mathcal{R}$ on superhorizon scales, which is given by

$$\mathcal{P}_{\mathcal{R},0}(k) = A_s \left(\frac{k}{k_*}\right)^{n_s-1}, \tag{1}$$

where A_s and n_s are the amplitude and the spectral index of the comoving curvature perturbations at a given pivot scale $k_* = 0.05$ Mpc^{-1}, we consider deviations as

$$\mathcal{P}_{\mathcal{R}}(k) = \mathcal{P}_{\mathcal{R},0}(k)[1 + \mathcal{P}_{\rm PF}(k)]. \tag{2}$$

There are many kinds of oscillatory patterns models such as features that oscillates linearly or logarithmically in k as well as oscillations with constant or scale-dependent amplitude [11,12,16,17,21–26,51–53]. We therefore consider the following templates with superimposed oscillations on the PPS,

$$\mathcal{P}_{\rm PF}(k) = \mathcal{A}_{\rm X} \sin(\omega_{\rm X}\Xi_{\rm X} + 2\pi\phi_{\rm X}), \tag{3}$$

where $\mathrm{X} = \{\mathrm{lin}, \log\}$ and $\Xi_{\rm X} = \{k/k_*, \log(k/k_*)\}$. These two templates with undamped oscillatory features (hereafter M1 and M2) are described by three extra parameters; an amplitude $\mathcal{A}_{\rm X}$, a frequency $\omega_{\rm X}$, and a phase $2\pi\phi_{\rm X}$ that we restrict to the range $[0, 2\pi]$. Linear extended oscillatory features can be generated by a sharp variation of background quantities $\propto \delta(\tau - \tau_0)$ where τ_0 determines the characteristic frequency of the oscillatory pattern. Such situations can be realized either by having sharp variation of the slow-roll parameters, induced for instance by a nonsmooth inflaton potential [11–15], or by sharp variation of the sound speed, induced for instance by a sudden turn in the multifield inflationary trajectory [22,54,55]. Alternatively, linear oscillatory features could arise assuming non-Bunch-Davies initial conditions; see Refs. [23–25]. Features with logarithmic oscillations can be generated when background quantities have an oscillatory time-dependent behavior themselves [56], such as models with periodic potentials [16,57,58]. Note that models cold also predict a scale-dependent amplitude for the oscillatory signal; see Refs. [11,23–25,37].

As third model (hereafter M3), we consider a localized bump [59]

$$\mathcal{P}_{\rm PF}(k) = \tilde{\mathcal{A}}_{\rm IR} \left(\frac{\pi e}{3}\right)^{3/2} \left(\frac{k}{k_{\rm IR}}\right)^3 e^{-\frac{\pi}{2}\left(\frac{k}{k_{\rm IR}}\right)^2} \left(\frac{k}{k_*}\right)^{1-n_s}, \tag{4}$$

described by two extra parameters; an amplitude that we rescale with the amplitude of comoving curvature perturbations $\tilde{\mathcal{A}}_{\rm IR} \equiv \mathcal{A}_{\rm IR}/A_s$ and a scale $k_{\rm IR}$ connected with the position of the bump. This feature is generated from particle production during inflation assuming a single burst of particles. Indeed, in models with a resonant production of particles the local interaction generates a bump in the PPS plus small linear oscillations which decay very quickly. We show the effect of the feature parameters on $\mathcal{P}_{\rm PF}(k)$ in Fig. 1.

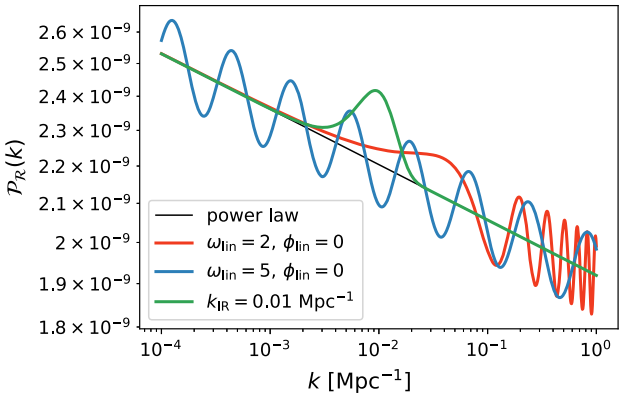

FIG. 1. PPS for the three templates analyzed. For M1 (red), we fix $\mathcal{A}_{\rm lin} = 0.05$, $\omega_{\rm lin} = 2$, and $\phi_{\rm lin} = 0$. For M2 (blue), we fix $\mathcal{A}_{\log} = 0.05$, $\omega_{\log} = 5$, and $\phi_{\log} = 0$. For M3 (green), we fix $\tilde{\mathcal{A}}_{\rm IR} \equiv \mathcal{A}_{\rm IR}/A_s = 0.1$ and $k_{\rm IR} = 0.01$ Mpc^{-1}.

III. DATA

In order to constraint these models, we consider the full DR12 data set[1] split into three redshift bins $0.2 < z < 0.5$, $0.5 < z < 0.75$, and (overlapping) $0.4 < z < 0.6$, following Ref. [60]. We study also the case combining the first two nonoverlapping redshift bins, neglecting their correlation.

We analyze the DR12 data set with the publicly available library `CosmoBolognaLib`[2] [61] by performing a Markov Chain Monte Carlo (MCMC) analysis.

For all redshift bins, we use the first two even multipole moments, i.e., the monopole and the quadrupole, of the anisotropic correlation function $\xi(s,\mu)$ measured using the minimum-variance unbiased estimator [62] with density-field reconstruction [63,64]

$$\xi(s,\mu) = \frac{DD(s,\mu) - 2DS(s,\mu) + SS(s,\mu)}{SS(s,\mu)}, \tag{5}$$

where DD, SS, and DS are the numbers of galaxy-galaxy, random-random, and galaxy-random pairs in bins of s and μ.

Unless otherwise noted, we use a flat ΛCDM cosmology given by $\Omega_{\rm m} = 0.31$, $\Omega_{\rm b}h^2 = 0.0220$, $h = 0.676$, $n_s = 0.97$, $\sigma_8 = 0.8$, and three massless neutrinos. This is consistent with *Planck* DR3 results [1] and is the same cosmological model as used in the papers studying the BOSS DR12 combined sample [60]. We consider the postreconstrunced

[1] https://data.sdss.org/sas/dr12/boss/papers/clustering/.
[2] https://gitlab.com/federicomarulli/CosmoBolognaLib.

galaxy 2PCF on the range of scales $20 < s\ [h^{-1}\,\mathrm{Mpc}] < 180$ divided in $\Delta s = 5\ h^{-1}\,\mathrm{Mpc}$ bins.

IV. ANISOTROPIC ANALYSIS OF THE BAO PEAK IN THE MULTIPOLES OF THE 2PCF

To build the model for the anisotropic 2PCF, we start modeling the nonlinear CDM power spectrum in redshift space [65–68]

$$P^{\mathrm{CDM}}(k,\mu) = [1+\beta\mu^2 R(k,\Sigma_r)]^2 F_{\mathrm{fog}}(k,\Sigma_s) P_{\mathrm{nw}}(k) \times [1 + P_{\mathrm{BAO}}(k) e^{-k^2\Sigma^2_{\mathrm{NL}}(\mu)/2}] \times [1 + P_{\mathrm{PF}}(k) e^{-k^2\Sigma^2_{\mathrm{PF}}/2}], \quad (6)$$

where

$$F_{\mathrm{fog}}(k,\mu,\Sigma_s) = \frac{1}{(1+k^2\mu^2\Sigma_s^2/2)^2} \quad (7)$$

$$P_{\mathrm{BAO}}(k) = \frac{P_{\mathrm{lin}}(k)}{P_{\mathrm{nw}}(k)} - 1 \quad (8)$$

$$\Sigma^2_{\mathrm{NL}}(\mu,\Sigma_\parallel,\Sigma_\perp) = \mu^2\Sigma_\parallel^2 + (1-\mu^2)\Sigma_\perp^2. \quad (9)$$

The linear power spectrum $P_{\mathrm{lin}}(k)$ is obtained with `CAMB`[3] [69,70] and the *no-wiggle* $P_{\mathrm{nw}}(k)$ is obtained with fitting formulae from Ref. [71], in both cases using our fiducial cosmology. β is the ratio between the linear growth rate $f(z) = \Omega_{\mathrm{m}}(z)^{0.545}$ and the linear clustering bias. We fix the streaming scale $\Sigma_s = 4\ h^{-1}\,\mathrm{Mpc}$. The radial and transverse components of the standard Gaussian damping of baryon acoustic oscillations (BAO) are fixed at $\Sigma_\parallel = 4\ h^{-1}\,\mathrm{Mpc}$ and $\Sigma_\perp = 2.5\ h^{-1}\,\mathrm{Mpc}$. $R(k,\Sigma_r) = 1 - e^{-k^2\Sigma_r^2/2}$ is the smoothing applied in reconstruction and $\Sigma_r = 15\ h^{-1}\,\mathrm{Mpc}$ is the smoothing scale used when deriving the displacement field [72]. Motivated by the weak dependence of current measurements of the 2PCF on the choice of damping scales (see Ref. [60]), we fix $\Sigma_{\mathrm{NL}} = \Sigma_{\mathrm{PF}}$. We test changing the fixed value of the Gaussian damping to $2\Sigma_{\mathrm{PF}}$, i.e. with a larger damping of the primordial features, finding negligible effects on the final constraints.

Following Refs. [60,73], we fit to the data using the following model for the monopole and quadrupole of the galaxy 2PCF

$$\xi_0(s) = B_0\xi_0^{\mathrm{CDM}}(s,\alpha_\perp,\alpha_\parallel) + A_0^0 + \frac{A_0^1}{s} + \frac{A_0^2}{s^2}, \quad (10)$$

$$\xi_2(s) = \frac{5}{2}[B_2\xi_2^{\mathrm{CDM}}(s,\alpha_\perp,\alpha_\parallel) - B_0\xi_0^{\mathrm{CDM}}(s,\alpha_\perp,\alpha_\parallel)] + A_2^0 + \frac{A_2^1}{s} + \frac{A_2^2}{s^2}, \quad (11)$$

[3] https://camb.readthedocs.io/en/latest/.

where $\xi_0^{\mathrm{DM}}(s,\alpha_\perp,\alpha_\parallel)$ and $\xi_2^{\mathrm{DM}}(s,\alpha_\perp,\alpha_\parallel)$ are the CDM 2PCF monopole and quadrupole computed at the fiducial cosmology, and $\{B_0, B_2, A_0^0 A_0^2, A_1^0, A_1^2, A_2^0, A_2^2\}$ are considered as nuisance parameters.

Given Eq. (6), we calculate the templates $\xi_0^{\mathrm{DM}}(s,\alpha_\perp,\alpha_\parallel)$ and $\xi_2^{\mathrm{DM}}(s,\alpha_\perp,\alpha_\parallel)$ starting from the definition of multipole moments

$$P_\ell(k) = \frac{2\ell+1}{2}\int_{-1}^{+1} \mathrm{d}\mu P(k,\mu) L_\ell(\mu), \quad (12)$$

where $L_\ell(\mu)$ are Legendre polynomials. These are transformed to 2PCF multipoles as

$$\xi_\ell(s) = \frac{i^\ell}{2\pi^2}\int \mathrm{d}k k^2 P_\ell(k) j_\ell(ks), \quad (13)$$

where $j_\ell(ks)$ is the ℓth order spherical Bessel function. We then use

$$\xi(s,\mu) = \sum_{\ell=0,2}\xi_\ell(s) L_\ell(\mu). \quad (14)$$

Finally, we take averages over μ

$$\xi_\ell(s,\alpha_\perp,\alpha_\parallel) = \int_{-1}^{1}\mathrm{d}\mu P_\ell(\mu_{\mathrm{true}})\xi(s_{\mathrm{true}},\mu_{\mathrm{true}}), \quad (15)$$

where $\mu_{\mathrm{true}} = \mu\alpha_\parallel/\sqrt{\mu^2\alpha_\parallel^2 + (1-\mu^2)\alpha_\perp^2}$, $s_{\mathrm{true}} = s\sqrt{\mu^2\alpha_\parallel^2 + (1-\mu^2)\alpha_\perp^2}$. All the nuisance parameters, i.e. B_0, B_2 and A_j^i, are used to marginalize over the clustering bias amplitude, redshift-space distortions, and the broadband effects including angle-dependent over all shape of the power spectra. We impose uniform flat prior on all parameters (see Table I for the prior ranges).

TABLE I. Priors for model parameters.

Parameter	Flat prior range
$\alpha_\perp, \alpha_\parallel$	[0.7, 1.3]
B_0, B_2	[0, 5]
$A_0^0, A_0^2, A_1^0, A_1^2$	$[-100, 100]$
A_2^0, A_2^2	$[-1000, 1000]$
$\mathcal{A}_{\mathrm{lin,log}}$	[0, 0.5]
$\tilde{\mathcal{A}}_{\mathrm{IR}}$	[0, 1]
ω_{lin}	[1.5, 13]
ω_{log}	[1, 50]
k_{IR} [Mpc^{-1}]	[0.001, 0.1]
$\phi_{\mathrm{lin,log}}$	[0, 1]

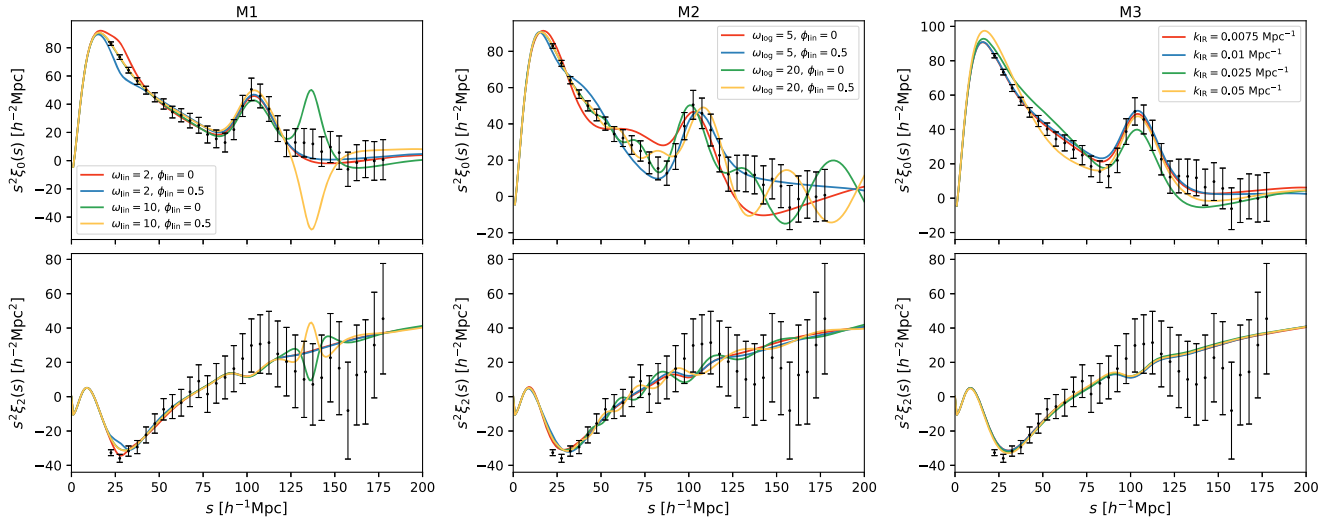

FIG. 2. Nonlinear galaxy 2PCF monopole (top panels) and quadrupole (bottom panels) computed at $z = 0.51$ for M1, M2, and M3 (from left to right). We fix the standard cosmological and model parameters to the baseline and we vary one feature parameter at a time. For M1 (left panel), we fix $\mathcal{A}_{\rm lin} = 0.05$ and we vary $\omega_{\rm lin} = \{2, 10\}$, $\phi_{\rm lin} = \{0, 0.5\}$. For M2 (central panel), we fix $\mathcal{A}_{\rm log} = 0.05$ and we vary $\omega_{\rm log} = \{5, 20\}$, and $\phi_{\rm log} = \{0, 0.5\}$. For M3 (right panel), we fix $\tilde{\mathcal{A}}_{\rm IR} \equiv \mathcal{A}_{\rm IR}/A_{\rm s} = 0.1$ and we vary $k_{\rm IR} = \{0.0075, 0.01, 0.025, 0.05\}$ Mpc^{-1}.

The effect of each of the feature parameters on the nonlinear galaxy 2PCF monopole and quadrupole is illustrated in Fig. 2 for a reference central redshift $z = 0.51$ of the BOSS DR12 sample. We see that M1 present a sharp peak or deep, depending on the value of the phase $\phi_{\rm lin}$, corresponding to the scale of the 2PCF located at $s \sim 20\omega_{\rm lin}$ Mpc. The signal is smoothed by nonlinear effects similarly to the case of the BAO [45,46], damping the primordial oscillations on the small scales of the Fourier space-matter power spectrum and leading to a broad bump on the 2PCF. Note that for $\omega_{\rm lin} \sim 7.5$ and $\phi_{\rm lin} = 0$ the peak coincides with the position of the BAO one, i.e., $s_{\rm BAO} \sim 150$ Mpc. M2 leaves a broad pattern on all scales in the 2PCF. Finally, we see, differently from what happened for the oscillatory templates, M3 generates a smooth and broad change of the 2PCF monopole shape. It is interesting to note that while the first two templates leave a clear oscillatory pattern also on the quadrupole, for the third model there is a negligible effect on the quadrupole.

V. RESULTS FOR THE ANISOTROPIC ANALYSIS

We start performing the standard BAO analysis on BOSS DR12 data for ΛCDM cosmology to validate our pipeline, using the measured postreconstructed monopole and quadrupole, for each redshift bin. Means and uncertainties for $\alpha_\perp$ and $\alpha_\parallel$, marginalized over $\{B_0, B_2, A_0^0 A_0^2, A_1^0, A_1^2, A_2^0, A_2^2\}$, agree well with the ones found in Ref. [60]; we collect the results in Table II. We repeat the BAO analysis in the presence of the template with linear oscillations (M1), logarithmic ones (M2), and a bump (M3). The constraints on $\alpha_\perp, \alpha_\parallel$ are affected in some cases by $< 20\%$ larger uncertainties, see Table II.

For M1, the marginalized 95% confidence limits (C.L.) upper bound on the amplitude of the primordial oscillations analyzing the 2PCF is $\mathcal{A}_{\rm lin} < 0.029$ at $z = 0.38$, $\mathcal{A}_{\rm lin} < 0.024$ at $z = 0.51$, $\mathcal{A}_{\rm lin} < 0.023$ at $z = 0.61$ on the frequency range $1.5 < \omega_{\rm lin} < 13$; combining the two nonoverlapping samples we obtain $\mathcal{A}_{\rm lin} < 0.025$ at 95% C.L. For M2, the marginalized 95% C.L. upper bound on the amplitude of the primordial oscillations is $\mathcal{A}_{\rm log} < 0.048$ at

TABLE II. Marginalized mean values and 68% C.L. for the 2D BAO parameters $\alpha_\perp$ and $\alpha_\parallel$ for the ΛCDM, M1, M2, and M3.

	ΛCDM		M1		M2		M3	
Sample	$\alpha_\perp$	$\alpha_\parallel$	$\alpha_\perp$	$\alpha_\parallel$	$\alpha_\perp$	$\alpha_\parallel$	$\alpha_\perp$	$\alpha_\parallel$
$0.2 < z < 0.5$	0.979 ± 0.014	1.017 ± 0.028	0.982 ± 0.017	1.004 ± 0.029	0.976 ± 0.015	1.022 ± 0.027	0.980 ± 0.014	1.015 ± 0.028
$0.4 < z < 0.6$	0.991 ± 0.014	0.988 ± 0.025	0.994 ± 0.016	0.989 ± 0.027	0.992 ± 0.014	0.986 ± 0.025	0.992 ± 0.014	0.988 ± 0.025
$0.5 < z < 0.75$	0.994 ± 0.023	0.953 ± 0.041	0.998 ± 0.024	0.948 ± 0.045	0.995 ± 0.025	0.950 ± 0.044	0.992 ± 0.021	0.957 ± 0.040
Combined	0.976 ± 0.014	1.031 ± 0.027	0.985 ± 0.018	1.017 ± 0.027	0.982 ± 0.016	1.016 ± 0.028	0.979 ± 0.014	1.018 ± 0.029

$z = 0.38$, $\mathcal{A}_{\log} < 0.023$ at $z = 0.51$, $\mathcal{A}_{\log} < 0.047$ at $z = 0.61$ on the frequency range $1 < \omega_{\log} < 50$; combining the two nonoverlapping samples we obtain $\mathcal{A}_{\log} < 0.027$ at 95% C.L. For M3, the marginalized 95% C.L. upper bound on the amplitude of the bump is $\tilde{\mathcal{A}}_{\rm IR} < 0.88$ at $z = 0.38$, $\tilde{\mathcal{A}}_{\rm IR} < 0.92$ at $z = 0.51$, $\tilde{\mathcal{A}}_{\rm IR} < 0.86$ at $z = 0.61$; combining the two nonoverlapping samples we obtain $\tilde{\mathcal{A}}_{\rm IR} < 0.34$ at 95% C.L. Constraints on the amplitude $\tilde{\mathcal{A}}_{\rm IR}$, derived using (4), depends on the details of the underlying model, in particular on the interaction term regulating the production of particles and the presence of a single or multiple bursts of particles. For a simple model where the inflation field ϕ interacts with the field χ through the Lagrangian term

$$\mathcal{L} = -\frac{g^2}{2}(\phi - \phi_0)^2\chi^2, \tag{16}$$

we can derive constraints on the coupling g thanks to the relation $\mathcal{A}_{\rm IR} \simeq 1.01 \times 10^{-6} g^{15/4}$ for a single burst of particle production during inflation [59]. We find for the combined sample $g^2 < 0.021$ at 95% C.L. (for $A_s = 2.1 \times 10^{-9}$), corresponding to a reasonable coupling values for models with phase transition during inflation and comparable in magnitude to the constraint obtained from CMB data in Refs. [59,74].

In Fig. 3, we show the comparison of the constraints on the feature parameters for all the three models studied for

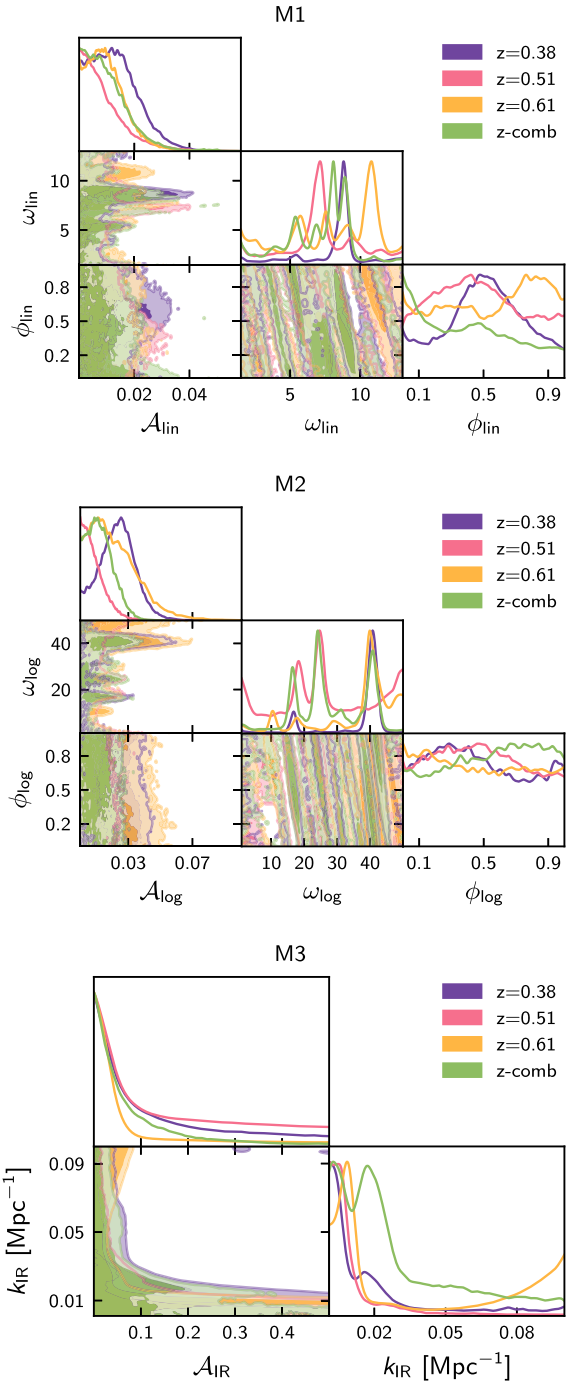

FIG. 3. Marginalized joint posterior distributions of the features parameters for M1, M2 and M3 models (from top to bottom).

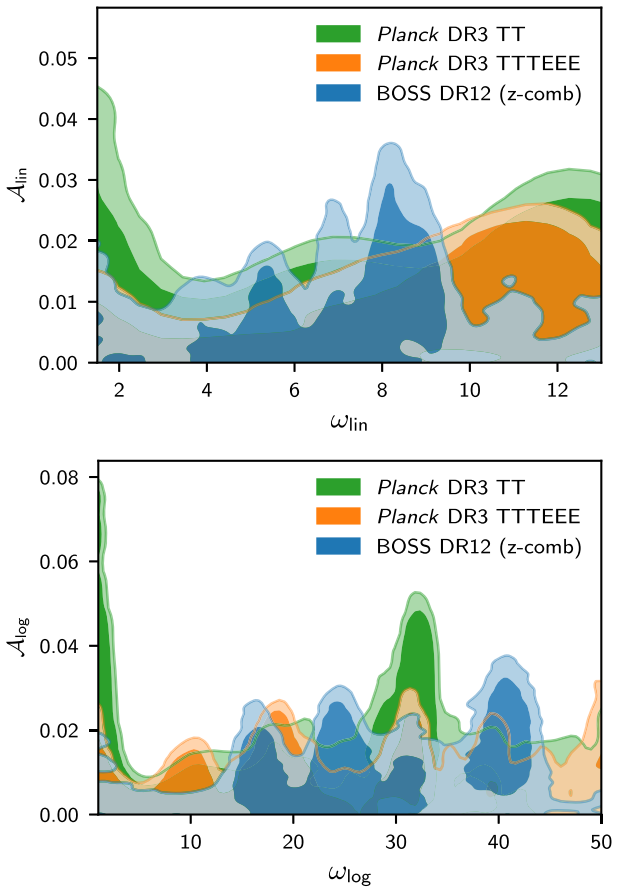

FIG. 4. Marginalized joint posterior distribution of the value of the feature parameters for M1 model (top panel) and M2 (bottom panel) obtained with the BOSS DR12 combined redshift bin and for the *Planck* DR3.

the BOSS DR12 single redshift analysis and the combined case.

The bounds on the first two templates with oscillatory features can be compared with the results inferred from CMB anisotropy observations obtained with *Planck* DR3 for the same templates [2]. The frequency coverage in the CMB analysis is wider for both templates, i.e., $1 < \omega_X < 10^{2.1}$. On the restricted frequency range covered by our analysis, the constraints from the 2PCF are comparable if not slightly tighter compared to the CMB ones. *Planck* DR3 constraints at 95% C.L. correspond to $\mathcal{A}_{\rm lin} < 0.029$ (< 0.028) for TT (TTTEEE) for M1 and $\mathcal{A}_{\rm log} < 0.043$ (< 0.023) for TT (TTTEEE) for M2. In Fig. 4, we overplot the marginalized posterior distribution on the feature amplitude depending on the frequency from our BOSS DR12 analysis with the one obtained from CMB *Planck* DR3. We are able to put tight constraints on some of the best-fit frequencies detected with CMB *Planck* data [2] using BOSS DR12 measurements. In particular, the best-fit for M1 from TTTEEE data corresponding to $\mathcal{A}_{\rm lin} = 0.015$ and $\omega_{\rm lin} \simeq 10$, and the best fit for M2 from TT data corresponding to $\mathcal{A}_{\rm log} = 0.024$ and $\omega_{\rm lin} \simeq 32$ are at odds with current LSS data.

Our constraints for M1 and M2 are consistent with the ones obtained in [45] where the same two templates have been constrained with the isotropic power spectrum monopole in Fourier space on the frequency ranges $5 < \omega_{\rm lin} < 45$ and $10 < \omega_{\rm log} < 80$, finding bounds on the features amplitude from BOSS DR12 up to a factor of 2.3 and 3.1 tighter than the ones obtained from CMB for $\omega_{\rm lin} > 10$ and $\omega_{\rm log} > 20$, respectively.

VI. CONCLUSIONS

In this paper, we have derived for the first time constraints on primordial feature in the PPS through the galaxy two-point correlation function. We have considered undamped superimposed oscillations, and a localized bump motivated by the production of particles during inflation. Our results show that the BOSS DR12 2PCF has the potential to achieve sensitivities competitive to current limits from *Planck* DR3 CMB anisotropies, improving the bounds on the average amplitude of such features and putting at odds some of the CMB best-fit frequencies found in *Planck* data. The complementarity between 2PCF and CMB measurements of primordial features opens exciting synergies, as verification of the primordial interpretation of anomalies in the CMB temperature and polarization angular power spectrum, that will lead the way to new studies of the physics of the early Universe.

Future galaxy clustering measurements, such as those expected from DESI [75], Euclid [76], SPHEREx [77], will significantly improve the current bounds obtained here in different aspects. Beyond a lower shot noise and higher redshift bins, a wider redshift volume will allow to probe larger separation scales and therefore target even higher frequencies for superimposed oscillations than those studied here.

ACKNOWLEDGMENTS

We all acknowledge financial support from the contract ASI/INAF for the Euclid mission No. 2018-23-HH.0. F. F. acknowledges support by the Agreement No. 2020-9-HH.0 ASI-UniRM2 "Partecipazione italiana alla fase A della missione LiteBIRD". L. M. acknowledges support from the Grant No. PRIN-MIUR 2017 WSCC32.

[1] N. Aghanim *et al.* (Planck Collaboration), Astron. Astrophys. **641**, A6 (2020); **652**, C4(E) (2021).
[2] Y. Akrami *et al.* (Planck Collaboration), Astron. Astrophys. **641**, A10 (2020).
[3] Y. Akrami *et al.* (Planck Collaboration), Astron. Astrophys. **641**, A9 (2020).
[4] A. A. Starobinsky, Phys. Lett. B **91**, 99 (1980).
[5] A. H. Guth, Phys. Rev. D **23**, 347 (1981).
[6] K. Sato, Mon. Not. R. Astron. Soc. **195**, 467 (1981).
[7] A. D. Linde, Phys. Lett. B **108**, 389 (1982).
[8] A. Albrecht and P. J. Steinhardt, Phys. Rev. Lett. **48**, 1220 (1982).
[9] S. W. Hawking, I. G. Moss, and J. M. Stewart, Phys. Rev. D **26**, 2681 (1982).
[10] A. D. Linde, Phys. Lett. **129B**, 177 (1983).
[11] A. A. Starobinsky, JETP Lett. **55**, 489 (1992).
[12] J. A. Adams, B. Cresswell, and R. Easther, Phys. Rev. D **64**, 123514 (2001).
[13] J. O. Gong, J. Cosmol. Astropart. Phys. 07 (2005) 015.
[14] X. Chen, R. Easther, and E. A. Lim, J. Cosmol. Astropart. Phys. 06 (2007) 023.
[15] D. K. Hazra, A. Shafieloo, G. F. Smoot, and A. A. Starobinsky, J. Cosmol. Astropart. Phys. 08 (2014) 048.
[16] X. Chen, R. Easther, and E. A. Lim, J. Cosmol. Astropart. Phys. 04 (2008) 010.
[17] R. Flauger, L. McAllister, E. Pajer, A. Westphal, and G. Xu, J. Cosmol. Astropart. Phys. 06 (2010) 009.
[18] D. J. H. Chung, E. W. Kolb, A. Riotto, and I. I. Tkachev, Phys. Rev. D **62**, 043508 (2000).
[19] A. E. Romano and M. Sasaki, Phys. Rev. D **78**, 103522 (2008).
[20] N. Barnaby, Z. Huang, L. Kofman, and D. Pogosyan, Phys. Rev. D **80**, 043501 (2009).
[21] X. Chen, Phys. Lett. B **706**, 111 (2011).
[22] X. Chen, J. Cosmol. Astropart. Phys. 01 (2012) 038.
[23] U. H. Danielsson, Phys. Rev. D **66**, 023511 (2002).
[24] R. Easther, B. R. Greene, W. H. Kinney, and G. Shiu, Phys. Rev. D **66**, 023518 (2002).

[25] J. Martin and R. Brandenberger, Phys. Rev. D **68**, 063513 (2003).
[26] X. Chen, A. Loeb, and Z. Z. Xianyu, Phys. Rev. Lett. **122**, 121301 (2019).
[27] H. V. Peiris *et al.* (WMAP Collaboration), Astrophys. J. Suppl. Ser. **148**, 213 (2003).
[28] P. A. R. Ade *et al.* (Planck Collaboration), Astron. Astrophys. **571**, A22 (2014).
[29] P. A. R. Ade *et al.* (Planck Collaboration), Astron. Astrophys. **594**, A20 (2016).
[30] G. Domènech, X. Chen, M. Kamionkowski, and A. Loeb, J. Cosmol. Astropart. Phys. 10 (2020) 005.
[31] R. E. Keeley, A. Shafieloo, D. K. Hazra, and T. Souradeep, J. Cosmol. Astropart. Phys. 09 (2020) 055.
[32] D. K. Hazra, A. Antony, and A. Shafieloo, J. Cosmol. Astropart. Phys. 08 (2022) 063.
[33] P. D. Meerburg, D. N. Spergel, and B. D. Wandelt, Phys. Rev. D **89**, 063537 (2014).
[34] R. Easther and R. Flauger, J. Cosmol. Astropart. Phys. 02 (2014) 037.
[35] X. Chen, M. H. Namjoo, and Y. Wang, J. Cosmol. Astropart. Phys. 02 (2015) 027.
[36] C. Zeng, E. D. Kovetz, X. Chen, Y. Gong, J. B. Muñoz, and M. Kamionkowski, Phys. Rev. D **99**, 043517 (2019).
[37] M. Braglia, X. Chen, and D. K. Hazra, J. Cosmol. Astropart. Phys. 06 (2021) 005.
[38] M. Braglia, X. Chen, and D. K. Hazra, Eur. Phys. J. C **82**, 498 (2022).
[39] M. Braglia, X. Chen, and D. K. Hazra, Phys. Rev. D **105**, 103523 (2022).
[40] Z. Huang, L. Verde, and F. Vernizzi, J. Cosmol. Astropart. Phys. 04 (2012) 005.
[41] X. Chen, P. D. Meerburg, and M. Münchmeyer, J. Cosmol. Astropart. Phys. 09 (2016) 023.
[42] X. Chen, C. Dvorkin, Z. Huang, M. H. Namjoo, and L. Verde, J. Cosmol. Astropart. Phys. 11 (2016) 014.
[43] M. Ballardini, F. Finelli, C. Fedeli, and L. Moscardini, J. Cosmol. Astropart. Phys. 10 (2016) 041; 04 (2018) E01.
[44] A. Slosar, K. N. Abazajian, M. Abidi, P. Adshead, Z. Ahmed, D. Alonso, M. A. Amin, B. Ansarinejad, R. Armstrong, C. Baccigalupi *et al.*, Bull. Am. Astron. Soc. **51**, 98 (2019).
[45] F. Beutler, M. Biagetti, D. Green, A. Slosar, and B. Wallisch, Phys. Rev. Res. **1**, 033209 (2019).
[46] M. Ballardini, R. Murgia, M. Baldi, F. Finelli, and M. Viel, J. Cosmol. Astropart. Phys. 04 (2020) 030.
[47] Z. Vlah, U. Seljak, M. Y. Chu, and Y. Feng, J. Cosmol. Astropart. Phys. 03 (2016) 057.
[48] A. Vasudevan, M. M. Ivanov, S. Sibiryakov, and J. Lesgourgues, J. Cosmol. Astropart. Phys. 09 (2019) 037.
[49] S. F. Chen, Z. Vlah, and M. White, J. Cosmol. Astropart. Phys. 11 (2020) 035.
[50] Y. Li, H. M. Zhu, and B. Li, Mon. Not. R. Astron. Soc. **514**, 4363 (2022).
[51] X. Wang, B. Feng, M. Li, X. L. Chen, and X. Zhang, Int. J. Mod. Phys. D **14**, 1347 (2005).
[52] R. Bean, X. Chen, G. Hailu, S. H. H. Tye, and J. Xu, J. Cosmol. Astropart. Phys. 03 (2008) 026.
[53] X. Chen, J. Cosmol. Astropart. Phys. 12 (2010) 003.
[54] A. Achucarro, J. O. Gong, S. Hardeman, G. A. Palma, and S. P. Patil, J. Cosmol. Astropart. Phys. 01 (2011) 030.
[55] X. Chen and Y. Wang, J. Cosmol. Astropart. Phys. 09 (2012) 021.
[56] R. Flauger and E. Pajer, J. Cosmol. Astropart. Phys. 01 (2011) 017.
[57] K. Freese, J. A. Frieman, and A. V. Olinto, Phys. Rev. Lett. **65**, 3233 (1990).
[58] L. McAllister, E. Silverstein, and A. Westphal, Phys. Rev. D **82**, 046003 (2010).
[59] N. Barnaby and Z. Huang, Phys. Rev. D **80**, 126018 (2009).
[60] A. J. Ross *et al.* (BOSS Collaboration), Mon. Not. R. Astron. Soc. **464**, 1168 (2017).
[61] F. Marulli, A. Veropalumbo, and M. Moresco, Astron. Comput. **14**, 35 (2016).
[62] S. D. Landy and A. S. Szalay, Astrophys. J. **412**, 64 (1993).
[63] D. J. Eisenstein, H. j. Seo, E. Sirko, and D. Spergel, Astrophys. J. **664**, 675 (2007).
[64] N. Padmanabhan, X. Xu, D. J. Eisenstein, R. Scalzo, A. J. Cuesta, K. T. Mehta, and E. Kazin, Mon. Not. R. Astron. Soc. **427**, 2132 (2012).
[65] N. Kaiser, Mon. Not. R. Astron. Soc. **227**, 1 (1987).
[66] K. B. Fisher, C. A. Scharf, and O. Lahav, Mon. Not. R. Astron. Soc. **266**, 219 (1994).
[67] X. Xu, N. Padmanabhan, D. J. Eisenstein, K. T. Mehta, and A. J. Cuesta, Mon. Not. R. Astron. Soc. **427**, 2146 (2012).
[68] X. Xu, A. J. Cuesta, N. Padmanabhan, D. J. Eisenstein, and C. K. McBride, Mon. Not. R. Astron. Soc. **431**, 2834 (2013).
[69] A. Lewis, A. Challinor, and A. Lasenby, Astrophys. J. **538**, 473 (2000).
[70] C. Howlett, A. Lewis, A. Hall, and A. Challinor, J. Cosmol. Astropart. Phys. 04 (2012) 027.
[71] D. J. Eisenstein and W. Hu, Astrophys. J. **496**, 605 (1998).
[72] H. J. Seo, F. Beutler, A. J. Ross, and S. Saito, Mon. Not. R. Astron. Soc. **460**, 2453 (2016).
[73] A. Veropalumbo, F. Marulli, L. Moscardini, M. Moresco, and A. Cimatti, Mon. Not. R. Astron. Soc. **442**, 3275 (2014).
[74] S. S. Naik, K. Furuuchi, and P. Chingangbam, J. Cosmol. Astropart. Phys. 07 (2022) 016.
[75] A. Aghamousa *et al.* (DESI Collaboration), arXiv:1611.00036.
[76] R. Laureijs *et al.* (Euclid Collaboration), arXiv:1110.3193.
[77] O. Doré, J. Bock, P. Capak, R. de Putter, T. Eifler, C. Hirata, P. Korngut, E. Krause, D. Masters, A. Raccanelli *et al.* (SPHEREX Collaboration), arXiv:1412.4872.